Biophysical *Journal*
Article

Biophysical Society

Two Cl Ions and a Glu Compete for a Helix Cage in the CLC Proton/Cl^- Antiporter

Cat Chenal[1] and M. R. Gunner[1,2,*]
[1]Biochemistry Ph.D. Program, The Graduate Center of the City University of New York and [2]Physics Department, The City College of New York of the City University of New York, New York, New York

ABSTRACT The ubiquitously expressed CLC chloride transporters are involved in a great variety of physiological functions. The CLC protein fold is shared by Cl^- channels and $2Cl^-$:$1H^+$ antiporters. The antiporters pump three charges per cycle across the membrane with two Cl ions moving in the opposite direction of one proton. Multiconformational continuum electrostatics was used to calculate the coupled thermodynamics of the protonation of the extracellular-facing gating Glu (E_x) and Cl^- binding to the external (S_x) and central (S_c) sites in CLC-ec1, the *Escherichia coli* exchanger. S_x, S_c, and E_x are buried within the protein where the intersection of two helix N-termini creates a region with a strong, localized positive potential for anion binding. Our chemical potential titrations describe the thermodynamic linkage for binding the Cl^- to each site and protons to E_x. We find that the $2Cl^-$:$1H^+$ binding stoichiometry is a result of Cl^- binding to S_x requiring H^+ binding to E_x, whereas Cl^- binding to S_c does not lead to proton uptake. When S_x binds a Cl^-, the protonated E_x moves upward, out of the positive helix cage. The increasing E_x proton affinity on binding the first Cl^- reduces the cost of binding the second Cl^- at either S_x or S_c. Despite the repulsion among the anions, the lowest energy states have two anions bound in the helix cage. The state with no Cl^- is not favored electrostatically, but relies on E_x blocking S_x and on the central residues Y445 and S107 blocking S_c.

INTRODUCTION

The CLC family of chloride channel proteins is a ubiquitously expressed group of homodimeric, proton-, and voltage-activated chloride transporters involved in a wide range of processes including ion homeostasis, renal endocytosis, bone resorption (1), and cell migration (2). The CLC family is split between passive ion channels and secondary-active Cl^-/H^+ antiporters (1), which maintain a $2Cl^-$:$1H^+$ stoichiometry of transport (3–6). X-ray structures of the *Escherichia coli* CLC exchanger, CLC-ec1, have provided insights into this unusual family and enabled detailed analysis of the connections between structure and function (7–9).

Each subunit of the CLC protein transports Cl^- independently (10–12) through a conduction pathway inferred from the locations of three Cl^- binding sites in the x-ray structures, denoted S_x, S_c, and S_i, for external, central, and intracellular site, respectively (7). The selectivity filter includes S_x and S_c. It is gated by a Glu, E_x (E148), which moves in and out of S_x (8), and by the central Ser and Tyr residues, Ser_c and Tyr_c (S107 and Y445) (13–15), which can occlude S_c (9). Moreover, as the Ala and Gln mutants (E148A, E148Q (8)) abolish H^+ transport while retaining Cl^- conduction (3,6,14), E_x is known to be the obligate proton donor/acceptor for the $2Cl^-$:$1H^+$ exchange.

S_x and S_c have a Cl^- affinity in the low millimolar range whereas that of S_i is >30 mM (9,16,17). S_x and S_c are ~4 Å apart in a helix cage binding site (18,19) located where the N-termini of helix F and helix N meet (7) (Fig. 1). The first two turns in these helical segments, which form the helix cage, were found previously to make a significant contribution to ion stabilization in both continuum electrostatics (19) and molecular dynamics (MD) simulations (20,21). The complex CLC protein fold is made up of an inverted topological repeat where two structurally similar halves are rotated ~180°. Here, the topology generates the helix cage anion binding sites. This particular fold occurs in many secondary-active transporters and enable the alternate-access mechanism (22,23). In this transport scheme, the substrate accessibility to one side of the membrane or the other is switched via coupled conformational changes of the extracellular and intracellular gates. Conformational changes are often divided into domain-level (or "heavy" gates) and residue-level ("light" gates) motions (note that in contrast to (24), we prefer "heavy" and "light" to the authors' "thick" and "thin"). Thus, in the CLC exchangers,

Submitted April 17, 2017, and accepted for publication July 11, 2017.
*Correspondence: mgunner@ccny.cuny.edu
Editor: Chris Chipot.
http://dx.doi.org/10.1016/j.bpj.2017.07.025

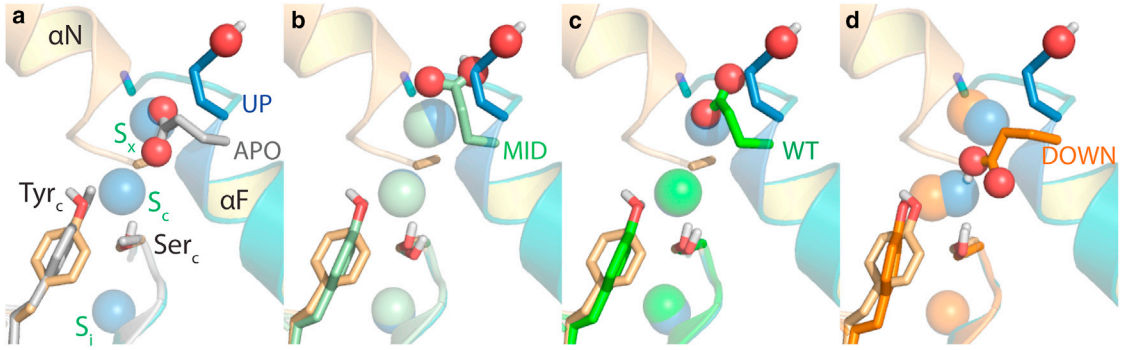

FIGURE 1 Anion binding site topology and position of key residues in CLC-ec1. Due to the inverted structural repeat in each subunit, the N-termini of α-helices F (αF, *teal*) and N (αN, *pale orange*) meet midmembrane and form an electropositive helix cage for anionic species, Cl^- and ionized E_x. CL_x, CL_c, and CL_i (*colored spheres*) are shown in binding sites S_x, S_c, and S_i. S_x and S_c are in the helix cage, whereas the low affinity intracellular binding site, S_i, is solution accessible (7). E_x, the gating Glutamate (E148), can occlude S_x and S_c, and the central Ser^{107} and Tyr^{445} (Ser_c and Tyr_c) can reach into S_c. Each panel depicts the position of E148Q mutant PDB: 1OTU (8) restored to Glu (UP structure, *blue*) together with (*a*) APO position, gray (PDB: 2EXW (9)). (*b*) MID position, light green (from PDB: 1OTS); (*c*) WT position, green (PDB: 1OTS (8)) and (*d*) DOWN position, orange (from PDB: 1OTS). Added CL_x in DOWN and MID structures comes from PDB: 1OTU. The ions have moved to slightly different positions in energy minimization (see Figs. S1 and S2).

E_x and Tyr_c and Ser_c would be the light gates, whereas changes in the helical domains to switch access to the inside or outside would be heavy gates. Exclusive binding of the two substrates was implied in the seminal, alternate-access transport paradigm (25), but later modified (24,26). CLC-ec1 experiments show that Cl^- and H^+ bind simultaneously and cooperatively (3,16,17), with the 2:1 stoichiometry of transport (17). The transport dynamics are consistent with the alternate-access mechanism (27), although it is not clear whether any of the alternate-access transport mechanism subtypes (22) are appropriate for the CLC exchangers.

The transmembrane domains of the crystal structures of all CLC exchangers are nearly identical. The main difference is the position of E_x, which can be grouped into four conformations. In WT CLC-ec1 (PDB: 1OTS (8)), the E_x side chain enters into S_x preventing Cl^- binding, so only S_c and low affinity S_i sites are filled. In the APO structure (PDB: 2EXW (9)), the E_x side chain reaches deeper into S_x, and Ser_c and Tyr_c are at the edge of S_c preventing Cl^- binding to either site. In the structure found in the red algae *Cyanidioschyzon merolae* (PDB: 3ORG (6)), the E_x side chain reaches downward into S_c, whereas S_x and S_i have Cl^- bound. Experiments on CLC proteins (28–30) and MD simulations (31–33) suggest that a downward conformation is part of the reaction cycle. Finally, 3 Cl^- are bound in the UP structure (PDB: 1OTU (8)) of the E148Q CLC-ec1 mutant where the Gln side chain is rotated up toward the extracellular solution. Recent experiments support the UP structure being in an outward facing and occluded orientation, which is not fully open to Cl^- entry from solution (27). E_x moves into the UP conformation in silico upon protonation of E_x in the wild-type protein (21,33,34).

MD simulations of CLC proteins have investigated the formation of water wires used for proton transfer (32,35), the coupling of water wires to the central site occupancy (36), and their disruption depending on the identity of the ion (37), which supports the experimental finding that the 2:1 stoichiometry of transport is disrupted if S_c is empty (38). Cl^- transport simulations have provided estimates for energetic barriers along the conduction pathway (21,31–35) and substrate binding affinities have been estimated via continuum electrostatic methods (19,39). However, to our knowledge, the thermodynamic linkage between the E_x and the two caged binding sites (S_x and S_c) has not been addressed in simulations.

In the work described here, a continuum electrostatics analysis is used to consider the thermodynamics of CLC-ec1 where three anions, E_x, CL_x, and CL_c, compete for sites that are close together. S_i is not considered due to its low affinity (9,16,17). This study provides the relative energy of the protein in states with different charges and describes how the protein supports binding of two closely spaced anions and only one proton, in a set of closely related structures, which differ primarily in the position of E_x. Our results indicate that: 1) the helix cage favors states with two anions, be they the ionized E_x carboxyl group or the Cl ions; 2) the E_x apo pK_a depends on the carboxyl group proximity to the positive backbone potential from the helix cage, which is focused at S_x; 3) E_x protonation is coupled to Cl^- binding to S_x only, regardless of the central site occupancy; and 4) the E_x pK_a increases with Cl^- bound in S_c, yet it remains ionized. Our main conclusion is that the electrostatics of the helix cage structure supports the 2:1 stoichiometry of binding.

MATERIALS AND METHODS

Simulation with the multiconformation continuum electrostatic program

The multiconformation continuum electrostatic (MCCE) program is a structure-based, continuum electrostatic and molecular mechanics program

that enables in silico titrations of protons and ions (40,41). MCCE samples multiple side-chain conformations given a fixed-backbone structure. Monte Carlo (MC) sampling finds the Boltzmann distribution of residue conformation together with ligand binding, and protonation states at a given pH, ionic strength, and ligand concentration. The proton affinity (pK_a) of each ionizable residue is determined from the pH dependence of the residue's protonation in MC sampling as a function of pH, whereas the K_d of a ligand is determined by changing the chemical potential of the ligand in solution. Calculations here use procedures previously applied to other Cl^- binding proteins (41,42) (see Supporting Material for further details).

Calculation of the proton affinity of the gating residue

Given the output from MC sampling, the aggregate factors shifting the energy of each group are estimated by a mean field energy analysis. Here the proton affinity is given as $pK'_{4.5}$, which is defined as the pH where the protonation free energy would be zero if the rest of the protein retains the equilibrium ionization and conformational states at pH 4.5 where the CLC-ec1 exchanger protein is maximally active (43),

$$pK'_{4.5} = pH_{4.5} - m\Delta G_{proton}/2.3RT, \quad (1a)$$

where m is 1 for acids and -1 for bases. ΔG_{proton}, the shift of the proton affinity for a residue or ligand due to the transfer from water to the protein, is broken down in MCCE as

$$-\Delta G_{proton} = 2.3RTm pK_{a,sol} + \Delta\Delta G_{dsol} + \Delta G_{bkb} + \Delta G_{tors} + \Delta G_{res,pH4.5} + T\Delta S, \quad (1b)$$

where $pK_{a,sol}$ is the solution pK_a of the residue or ligand, $\Delta\Delta G_{dsol}$ is the loss of solvation energy, ΔG_{bkb} is the interaction with the backbone amides, ΔG_{tors} is the torsion energy, $\Delta G_{res,\ pH4.5}$ is the residue pairwise interaction energy with other residues equilibrated at pH 4.5, and $T\Delta S$ is an entropy correction term (40). Thus, when MC sampling shows E_x fully protonated or deprotonated at pH 4.5, $pK'_{4.5}$ provides an estimate of the free energy of changing protonation state. The MFE values are an approximation as they fix the protein residues in the equilibrium conformation, so they do not contain the work needed to make other changes throughout the protein when E_x titrates, which is captured in the free MC titration (44) (Fig. S4).

Structure preparation

Three CLC crystal structures were subjected to energy minimization with different combinations of bound Cl^- ions and with conformationally distinct E_x (E148) positions to generate structures designated APO, WT, MID, UP, and DOWN (Fig. 1; Table S1). The work presented here evaluates how the position of E_x and mutants of this Glu determines the stoichiometry and energy of Cl^- and proton binding. The APO protein structure (PDB: 2EXW), has E_x in the S_x binding site and the side chains of Ser_c and Tyr_c in S_c. WT is the wild-type protein (PDB: 1OTS) with 2 Cl^- ions bound in the x-ray structure at S_c and S_i and the E_x OE1 atom <1 Å away from the empty S_x binding site. The MID structure was derived here from PDB: 1OTS to accommodate a Cl^- ion in S_x by moving the E_x side chain (Fig. 1; Table S1); the MID E_x OE1 atom is ~3 Å away from S_x. The UP structure (reversed mutation in the E148Q PDB: 1OTU structure (8)) has E_x OE1 in the UP position ~6 Å from S_x and ~4 Å from the E_x termini in the APO structure. Structures with E_x pointing inward (DOWN) were generated from PDB: 1OTS to replicate its conformation in the *C. merolae* structure (PDB: 3ORG (6)). This E_x side chain is ~3 Å from S_x (Fig. S2). Movement of E_x into the DOWN conformation does not exclude CL_c (Fig. 1) as it does in the PDB: 3ORG structure. Instead, E_x lies between the two Cl^- binding sites. This is also found in MD simulations that start from the PDB: 1OTS structure (32). The difference in E_x positions may result from a substitution of Arg^{147} in *E. coli* to Trp in *C. merolae* or a downward tilt of αF (Fig. S2).

All structures were subjected to GROMACS energy minimization (45,46) with three Cl^- ions, except for APO (PDB: 2EXW (9)), which was kept in the apo state. (The details of the minimization step are in Supporting Material.) The position of the Cl^- bound at the external site is taken from PDB: 1OTU (8) when it was not present in the input structure. Missing residues, all far from the binding sites, were not replaced. In silico mutations were made with the side-chain completion algorithm in MCCE before GROMACS energy minimization.

RESULTS

The Cl^- affinities at the external (S_x) and central (S_c) sites and their dependence on the proton affinity of E_x, the external side gating Glu^{148}, were determined. The analysis primarily compares the behavior of the structures with E_x in the UP and MID structures, focusing on the free energy of the states with 0, 1, or 2 Cl^- in the presence of an ionized or protonated E_x. The MID structure has E_x in a position near S_x, which does not clash with a Cl^- bound in that site. The proton affinity of E_x and Cl affinity to the two binding sites in individual structures and those with E_x mutated to Gln or Ala are found in Tables S2–S5.

Thermodynamic relationship between the E_x proton affinity and Cl^- affinity of S_x

The proton affinity of E_x in the absence of Cl^- is strongly correlated with its position (Fig. 2 *a*; Tables 1, and S2). The average apo $pK'_{4.5}$ value is negative wherever E_x is close to S_x: it is -6 in the APO structure, -7 in WT, -4 in DOWN, and -3 in MID, whereas it is three in the UP structure. Thus, E_x remains ionized in the absence of Cl^-. However, the simple movement of E_x away from S_x in the generally static protein structures investigated here leads to a remarkable change in the apo protein proton affinity of ~12 kcal/mol. The source of this variation will be described below.

Cl^- chemical potential titrations were performed at pH4.5, with all residues free to titrate and explore different rotamers on the fixed protein backbone (Fig. 2 *c*, *d*, and *e*). E_x protonation is tightly coupled to CL_x binding (Fig. 2, *a* and *b*). In all cases, E_x is fully protonated in the presence of CL_x and almost always fully ionized in its absence. There are small changes in protonation throughout the protein, but E_x is the sole residue that shows a consistent, significant change in protonation when Cl^- binds to S_x.

The proton coupled Cl^- affinity for S_x varies by 20 kcal/mol among the different structures (Table S2), which are very similar except for the position of E_x. The energy of the coupled binding reaction can be dissected using a thermodynamic cycle. This explicitly considers that the energy needed to protonate E_x at pH 4.5 (Eq. 1 *a*) adds a

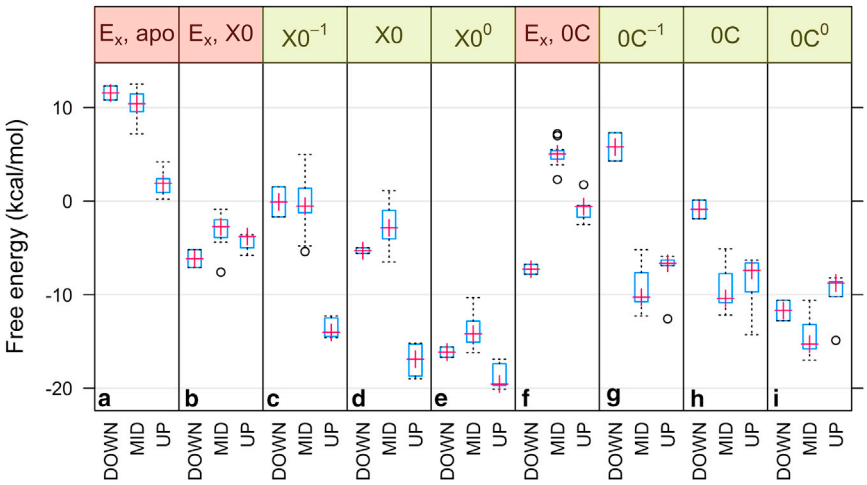

FIGURE 2 Free energy of E_x protonation and Cl^- binding at S_x and S_c. Given here is the free energy of E_x protonation (*a*) with no Cl^- bound; (*b*) with CL_x bound; (*f*) with CL_c bound. Note that positive values favor ionized E_x. Given here is relative free energy of Cl^- binding at S_x (S_c empty) with: (*c*) E_x fixed ionized; (*d*) E_x free to titrate; (*e*) E_x fixed neutral; or at S_c (S_x empty) with: (*g*) E_x fixed ionized; (*h*) E_x free to titrate; (*i*) E_x fixed neutral. The box height encloses 50% of the values (interquartile range, 25%, 75%); here, the upper (*lower*) dashed bar indicates the highest (*lowest*) value within 1.5 interquartile range; the plus sign indicates the average; and small circles indicate outliers. The individual data points are in Tables S2 and S3. To see this figure in color, go online.

penalty to S_x binding, which can be substantial when the E_x proton affinity is low. In Fig. 3 paths, *A* and *A′* represent the proton binding to E_x in the apo or Cl^- bound state. Paths *B* and *B′* represent the Cl^- binding to S_x when E_x is fixed neutral (ΔG_b^n) or ionized (ΔG_b^i). Path *C* is the coupled H^+/Cl^- binding reaction when both ligands are free to titrate (ΔG_b^{free}). Relative Cl^- binding energies for paths *B*, *B′*, and *C* are obtained from the binding curves computed by the grand canonical Monte Carlo (MC) simulation of the Cl^- binding as a function of the chemical potential where all groups remain at equilibrium with the bound ion. The proton affinity of E_x (ΔG_{proton}, paths *A* and *A′*) is computed with the mean field energy approach keeping all other ionizable residues fixed in their equilibrated state at pH 4.5 (Eq. 1). In MID structures, the lower energy path greatly favors protonating E_x before S_x is bound. In the UP structures where the E_x pK_a is near 4.5, the intermediates where the proton or the Cl^- bind first have similar energy.

The Cl^- affinity of S_x, ΔG_b^{free}, is correlated with the energy required to bind a proton to E_x in the apo state because binding proton and Cl^- are strongly coupled (Fig. 4; Table S2). Yet, even with a neutral E_x (ΔG_b^n), S_x binds Cl^- ~5 kcal/mol more tightly in the UP structures, indicating that other structural differences between the WT PDB: 1OTS and the E148Q PDB: 1OTU structures influence the Cl^- affinity to S_x.

The proton-coupled Cl^- affinity between E_x and S_x is also seen when we consider the difference between the average affinities in structures that were energy minimized with E_x neutral versus those that were energy minimized with E_x ionized: in MID, the small difference in proton affinity in the apo state (1.3 kcal/mol) is also the difference in ΔG_b^{free}, and similarly in UP with values of −2.1 and −2.7 kcal/mol, respectively. This check also supports E_x as being the obligate proton Glutamate of the extracellular side (3,6,14)

TABLE 1 Nomenclature for Titrations

Titration Identifier	Titrating Group: Site(s)/E_x	Ion Titrating	Initial State	Final State
X0	S_x alone/E_x free to titrate	CL_x	00	10
$X0^{charge}$	S_x alone/E_x charge fixed	CL_x	00^{charge}	10^{charge}
X1	S_x with fixed CL_c/E_x free to titrate	CL_x	01	11
$X1^{charge}$	S_x with fixed CL_c/E_x charge fixed	CL_x	01^{charge}	11^{charge}
0C	S_c alone/E_x free to titrate	CL_c	00	01
$0C^{charge}$	S_c alone/E_x charge fixed	CL_c	00^{charge}	01^{charge}
1C	S_c with fixed CL_x/E_x free to titrate	CL_c	10	11
$1C^{charge}$	S_c with fixed CL_x/E_x charge fixed	CL_c	10^{charge}	11^{charge}
XC	S_x and S_c/E_x free to titrate	CL_x CL_c	00	11

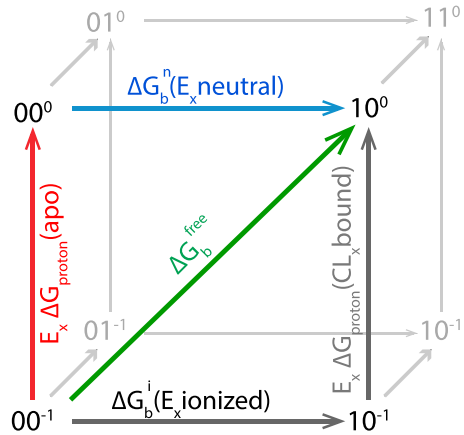

FIGURE 3 Thermodynamic cycle for eight states in proton-coupled Cl^- binding for the three anions (CL_x, CL_c, and E_x) competing for the helix cage. (*Front face*) Protonation of E_x is coupled to the binding of CL_x. Vertices indicate bound states. (*Vertical arrows*) H^+ affinity of E_x in the apo (00, *left*), or CL_x bound state (10, *right*). (*Horizontal arrows*) CL_x binding when E_x is fixed neutral (ΔG_b^n, *top*), or ionized (ΔG_b^i, *bottom*). (*Diagonal*) Coupled H^+ and CL_x binding with E_x free to titrate (ΔG_b^{free}). Path via 00° is favored by 14 (±3) kcal/mol in the ensemble of MID structures and by 4 (±3) kcal/mol in UP structures. (*Back face*) Shown here are states with CL_c bound. Values for each leg of the cube in the MID and UP structures are given in Table S8. To see this figure in color, go online.

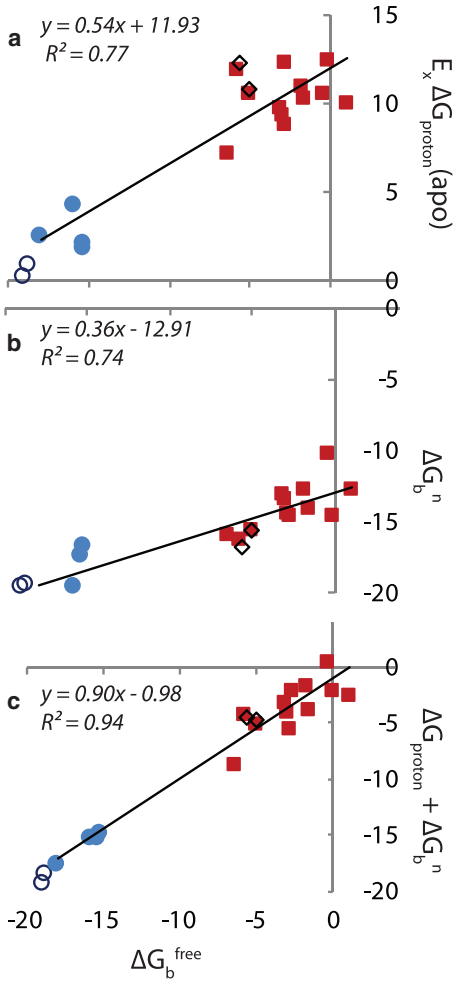

FIGURE 4 Thermodynamic linkage of the energy of CL_x binding and E_x protonation. Given here is the proton-coupled Cl^- binding affinity, ΔG_b^{free} (*diagonal path*; Fig. 3) versus (*a*) the energy to protonate E_x, in the apo state, $\Delta G_{proton.}$ (*left path*); (*b*) the relative Cl^- binding affinity of S_x when E_x is fixed neutral, ΔG_b^n (*top path*); and (*c*) $\Delta G_{proton.}+\Delta G_b^n$. (*Solid red squares*) Given here are MID structures and (*diamonds*) DOWN structures. (*Solid blue circles*) Given here are UP structures with E_x ionized during energy minimization and (*open blue circles*) UP structures with E_x neutral during energy minimization, which are excluded from best fit because they are partially protonated in the apo state. Negative free energies stabilize protonation of E_x and binding of Cl^-.

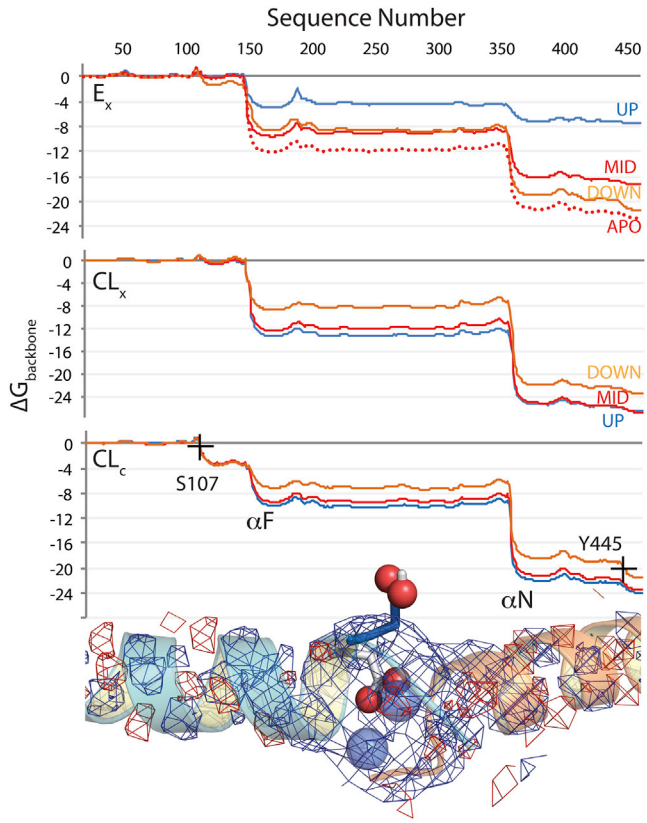

FIGURE 5 Running sum of the energy of interaction between the backbone and either E_x, CL_x, or CL_c. (*Top*) Given here is E_x in four structures without Cl ions; (*middle*) CL_x; and (*bottom*) CL_c. The two large drops in the energy identify two stabilizing motifs forming the helix cage: αF, the E_x motif (N-terminal end of helix F, colored *teal* in the image), $L^{145}G^{146}R^{147}E^{148}G^{149}P^{150}xxV^{152}$; and αN, the F357 motif (N-terminal end of helix N colored *orange* in the image) $G^{354}G^{355}I^{356}F^{357}A^{358}xM^{360}$. The Cl ions are almost equally stabilized by the helix cage, but at CL_c the positive potential further gains from backbone elements around the inner gate residues Ser_c (S107) and Tyr_c (Y445). The image shows the superimposed conformations of E_x in APO (*gray*) and in UP (*blue*) together with the ± 15 kcal/mol electrostatic potential envelope (*red*, negative; *blue*, positive) calculated from the APO backbone elements. E_x in APO or the Cl ions when bound, are inside the electropositive cage, whereas E_x in UP is outside.

because only the charge of E_x is different in the differently energy-minimized structures.

Structural determinants of E_x apo pK_a and Cl^- affinity

The protein as a whole influences the Cl^- and proton affinity. The loss of solvation energy favors protonation of a buried Glu and release of the chlorides. The dimeric CLC-ec1 has a net charge of +32 so interactions with the residues favor the anionic E_x and Cl^- binding. However, these energies vary little among the MID, UP, and other structures studied here (Fig. S5). The protein backbone dipoles form a helix cage (18,19) that stabilizes E_x ionization and Cl^- binding at S_x or S_c (Fig. 5). The differences in backbone interaction energy with E_x accounts for most of the 12 kcal/mol variation of the proton affinity in the different structures (Fig. S6). In contrast, the positive potential favoring binding of CL_x by -26 ± 1 kcal/mol and CL_c by -24 ± 1 kcal/mol varies little between structures.

The backbone interaction energy plotted as a running sum (Fig. 5) identifies two regions that stabilize E_x, the external and central sites. One is the N-terminal end of helix F, which flanks the gating Glu, $G^{146}xE^{148}G^{149}P^{150}$, and the other is the N-terminal end of helix N, which includes the conserved sequence F^{357}, $G^{355}xF^{357}xP^{359}$ (with *x* denoting a nonconserved position) (Fig. S1 *b*). The positive potential comes from the first two turns of each helix. The inverted topological repeat of the CLC fold generates the binding site, as the N-terminal ends of helix F and helix N meet near the

midpoint of the membrane to create the electropositive hot-spot for two negative charges (39) (Figs. 1 and S1 *b*). S_c, which is slightly offset from the region of maximum potential from the helices, also relies on the backbone elements of the inner gate residue motifs, Ser_c and Tyr_c (*c* and *d* in Fig. 5).

Use of backbone elements creates a site with interesting properties. Although the N-terminal sequences of these helices are highly conserved, the electrostatic potential is relatively independent of the side-chain identity. The stabilization by helical N-termini means that the groups that attract the Cl^- ions cannot participate in coupled proton binding, so they provide stabilization in a manner that does not conserve charge and can be pH independent; and lastly the potential created by the dipoles is focused in a small region. Therefore, small movements of Cl^- or E_x relative to the center of the helix cage leads to very significant changes in proton or Cl^- affinity (Figs. S1 and S6).

Thermodynamic relationship between the E_x proton affinity and the S_c affinity for Cl^-

The binding affinity of Cl^- to S_c was obtained keeping S_x empty with E_x fixed neutral, charged, or free to titrate (Fig. 2; Table 3). On average, Cl^- binds S_c with similar affinity in the UP and MID structures. CL_c raises the E_x proton affinity by 5 kcal/mol in the MID structures and by 3 in the UP structures. As the E_x pK_a is near pH 4.5 in the UP structure apo state, E_x begins to protonate in the presence of CL_c even when S_x is empty. In the WT or MID structures, CL_c shifts the E_x pK_a up but not enough to lead to proton binding (Table 2). However, as will be seen, the increase in the proton affinity in the presence of CL_c reduces the free energy needed for the subsequent proton coupled Cl^- binding at S_x. In addition, the side chains of Ser_c and Tyr_c will often rotate into the unbound central site. The work needed to displace them stabilizes the APO state underlying their role as intracellular side-gating elements (13–15).

TABLE 2 Proton Affinity of E_x in States with Different Chloride Occupancy

	$\Delta G_{proton.} \pm$ SD (kcal/mol)				$PK'_{4.5}$			
Type	apo	X0	0C	XC	apo	X0	0C	XC
APO	14 ± 2				−6			
UP	2 ± 1	−4 ± 1	−1 ± 1	−5 ± 1	3	7	5	8
MID	10 ± 2	−3 ± 2	5 ± 1	−9 ± 2	−3	7	1	11
DOWN	12 ± 1	−6 ± 1	−7 ± 1	−22 ± 1	−4	9	10	21

The proton affinity of E_x. Type denotes the structure named after its E_x position (Fig. 1 and Table S1). See Table 1 for definition of titrations. ΔG_{proton} was calculated with the mean field energy approximation (Eq. 1) at pH 4.5 and averaged for each structure type and fixed Cl^- occupancy. Values for subunits A and B are averaged together. Cl^- occupancy: apo (no Cl^-), X0 (CL_x), 0C (CL_c), XC (both CL_x and CL_c). Positive values of ΔG_{proton} favor ionized E_x. Individual values for all structures are given in Tables S2–S4.

Binding to S_x and S_c with E_x in the DOWN conformation

E_x has also been found in a position between the two Cl^- binding sites in the DOWN position (Fig. S2 *a*). In moving from UP to DOWN position, the E_x residue may be a baton in the 15 Å proton-relay between the intra- and extracellular compartments. In the DOWN structure, Cl^- binding at either S_x or S_c leads to E_x protonation. Thus, if a proton is bound along with CL_x it will remain bound if E_x moves DOWN as the Cl^- moves to S_c.

Thermodynamic relationship between the proton affinity and relative Cl^- affinity at S_x and S_c in two-site titrations

CL_x and CL_c are only 4 Å apart. The pairwise Cl^-:Cl^- repulsion amounts to ~15 kcal/mol and creates a challenge for simultaneous Cl^- binding (Table S6). However, the helix cage creates a region of extreme positive potential stabilizing each ion by ~25 kcal/mol (Fig. 5), which is larger than the ion-ion repulsion and permits the two charges to bind.

When both sites titrate freely (Table 2, XC), the site with the strongest Cl^- affinity in the single site titration in a given structure is filled first with a ΔG_b similar to that found in the single site titration. A higher Cl^- concentration is then required to fill the second site. The affinity of the second Cl^- for the helix cage might be expected to be simply the Cl^- affinity of the apo protein weakened by the pairwise Cl^-:Cl^- repulsion (Fig. 6). However (using the MID structure as an example), the binding of CL_x is weakened by only ~7 kcal/mol in the presence CL_c relative to a titration without CL_c ($\Delta G_{b,rel}$ for X0 versus X1; Table 3). Likewise, binding CL_x with CL_c present is the same 7 kcal/mol weaker ($\Delta G_{b,rel}$ for 0C versus 1C; Table 3). Thus, the affinity is (15,7) = 8 kcal/mol higher than expected. The interaction of the CL with E_x is the source of this positive cooperatively in the binding of two Cl^- as described in the expressions in Eq. 2:

$$\begin{aligned}\Delta G_b(X0) &= \Delta G_b(OO \rightarrow XO)\\ &= \Delta G_b\left(XO^0\right) + \Delta G_{\text{proton.}}(OO),\end{aligned} \qquad (2a)$$

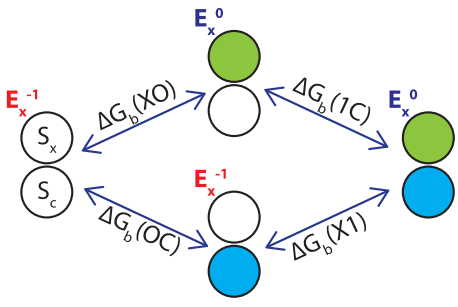

FIGURE 6 The thermodynamic coupling between proton and Cl^- binding. Open circles depict empty sites. Eq. 2 describes energies for each leg of the box. To see this figure in color, go online.

TABLE 3 Relative Cl^- Affinities of S_x and S_c at pH 4.5

		$\Delta G_{b,rel}$ ± SD (kcal/mol)						
Site	Type	X0	$X0^0$	$X0^{-1}$	X1	$X1^0$	$X1^{-1}$	XC
S_x	UP	−17 ± 2	−19 ± 1	−14 ± 1	−6 ± 1	−6 ± 1	−1 ± 1	−17 ± 2
	MID	−3 ± 2	−14 ± 2	0 ± 3	4 ± 3	0 ± 3	13 ± 3	3 ± 4
	DOWN	−5 ± 0	−17 ± 2	0 ± 2	−6 ± 2	−6 ± 1	9 ± 2	−4 ± 0
Site	Type	0C	$0C^0$	$0C^{-1}$	1C	$1C^0$	$1C^{-1}$	XC
S_c	UP	−9 ± 3	−10 ± 3	−8 ± 3	2 ± 2	2 ± 2	5 ± 2	2 ± 2
	MID	−9 ± 2	−15 ± 2	−9 ± 2	−2 ± 2	−2 ± 2	4 ± 2	−9 ± 4
	DOWN	−1 ± 1	−12 ± 2	6 ± 2	−1 ± 3	−1 ± 2	>10	−1 ± 2

The relative Cl^- affinity ($\Delta G_{b,rel}$) of S_x and S_c at pH 4.5 per structure type and E_x charge and Cl site occupancy. XC allows Cl^- to bind to either site. (*Top*) CL_x affinity; (*bottom*) CL_c affinity. In UP structures, CL_x binds more tightly so Cl_c binds in the presence of CL_x, whereas in MID structures, CL_c has higher affinity so CL_x affinity reflects the presence of CL_c.

$$\Delta G_b(0C) = \Delta G_b(OO \rightarrow OC) = \Delta G_b\left(OC^0\right) + \Delta G_{\text{repuls.}}\left(E_x^- : CL_c\right), \quad (2b)$$

$$\Delta G_b(1C) = \Delta G_b(XO \rightarrow XC) = \Delta G_b\left(OC^0\right) + \Delta G_{\text{repuls.}}(CL_x : CL_c), \quad (2c)$$

$$\Delta G_b(X1) = \Delta G_b(OC \rightarrow XC) = \Delta G_b\left(X0^0\right) + \Delta G_{\text{repuls.}}(CL_x : CL_c) + \Delta G_{\text{proton.}}(OC), \quad (2d)$$

$$\Delta G_{\text{proton.}}(OC) = \Delta G_{\text{proton.}}(OO) - \Delta G_{\text{repuls.}}\left(E_x^- : CL_c\right). \quad (2e)$$

E_x creates a penalty for binding the first Cl^- ($\Delta G_{repuls.}$; Eq. 2). When only S_c is bound, E_x remains ionized, repelling CL_c by 7 kcal/mol (Eq. 2 *b*). If CL_x has bound first, E_x is now protonated, so CL_c is repelled by CL_x but not by E_x (Eq. 2 *c*). Alternatively, the binding of CL_x is strongly coupled to E_x protonation, in a system where the starting proton affinity is very low (Eq. 2 *a*). The presence of a first bound CL_c raises the proton affinity of E_x by 5 kcal/mol (Eq. 2 *e*), diminishing the energy needed for the proton-coupled CL_x binding. Thus, the presence of E_x weakens the affinity of the first Cl^- bound (Eq. 2 *a* and *b*), but makes it relatively easier to bind the second anion. The protonation of E_x accounts for five of the 7 kcal/mol, whereas fractional changes in protonation of other more distant sites coupled to whichever Cl ion binds first accounts for the remaining 2 kcal/mol. In the UP state, the interaction of E_x with the bound Cl^- is smaller, contributing only 3 kcal/mol to the binding energies.

The relative energy of the eight different states for the coupled proton and Cl^- binding in the MID and UP structures is summarized in Fig. 7. The apo state with E_x ionized (00^-) is used as the reference. Values for structures with different E_x are derived from different crystal structures and have been computed and averaged separately. The energy between (00^-) in MID to UP conformations is ~12 ± 3 kcal/mol. The overall conclusion is that the state with the lowest energy has two anions. In the MID structures, the lowest energy state is 01^-. This is the configuration found in the WT PDB: 1OTS structure, which has a Cl^- in S_c, and the side chain of E_x remains in the positive helix cage. When E_x has rotated out of the helix cage to the UP position, the lowest energy state is 11°, with two Cl and a protonated E_x. This is consistent with the Cl^- occupancy and gating residue position in the E148Q mutant structure PDB: 1OTU. Other combinations of states are clustered at energies that depend on the E_x position. MID states with both CL_x and E_x^{-1} are highly destabilized. Thus, binding to S_x is strongly coupled to proton binding. In UP structures, states with 1 or 2 Cl^- bound differ by, at most, 5 kcal/mol.

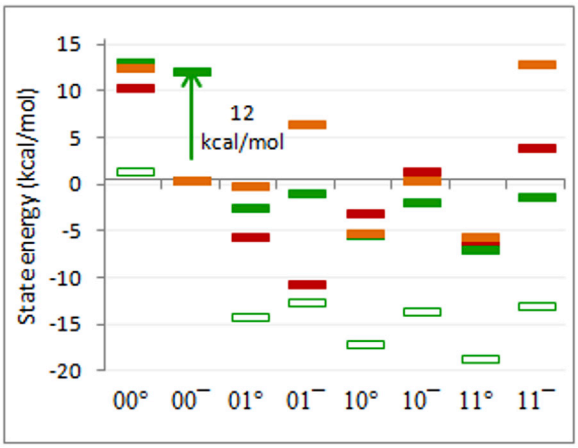

FIGURE 7 Relative energy of the eight states for binding CL_x, CL_c, and protonating E_x of CLC-ec1 at pH 4.5 (Table S7). The *x* axis identifies the state: first digit, S_x; second digit, S_c. The superscript is the charge of E_x. (*Red*) MID; (*green*) UP; (*orange*) DOWN. The energy at 00^{-1} is taken as the reference for both structures. (*Open green dashes*) Shown here is the energy independently calculated in the MID and UP structures. (*Solid green markers*) These symbols account for an ~12 kcal/mol cost to move from MID to UP structures in the 00^{-1} state.

Thus, it is easier to move Cl^- between sites in UP structures. In UP structures, the energies of states with E_x protonated are 2–5 kcal/mol lower than with the Glu ionized, showing the propensity of the Glu to remain protonated when it is out of the helix cage. The electrostatic energy of the apo state 00^{-1} is substantially higher than states with two charges. The light gates in S_x (E_x) and in S_c (Tyr_c and Ser_c) appear to be needed to stabilize the apo state. The similarity of the 00° and 00^{-1} states in UP reflects the pK_a being ~4.5 in this configuration.

DISCUSSION

The calculations investigate the affinity of the Sx and Sc binding sites for the external and central Cl^- (CLx and CLc) and the proton affinity of the gating Glu, E_x, in different positions in the whole protein in a membrane of low dielectric constant. Our findings provide a semiquantitative explanation at the atomic level for existing experimental data for the behavior of the structures in the Cl binding stage of the reaction cycle. In the absence of CLx, Ex binds very close to Sx (APO structure). When Ex is neutral, it moves up, as seen in the E148Q mutant structure, which is used to generate UP structures here. MID structures are prepared with E_x near S_x, without directly clashing with CL_x. Here an ionized E_x retains a strong electrostatic attraction for the helix cage and repulsion with CL_x, but does not have the extremely large van der Waals clash found between E_x in an APO structure with an introduced CL_x. Similar positions have been investigated in earlier MD simulations (19). In the absence of Cl^-, the ionized E_x in the APO structure is stabilized by ~4 kcal/mol more than in in MID structures. Thus, MID structures underestimate the energy required to protonate E_x when CL_x binds. However, consideration of E_x in the MID and UP as well as APO and DOWN structures allows a more complete, if qualitative picture of the relative free energies of the states with different Cl^- occupancies and E_x position and charge.

The characteristics of the CLC binding affinities that emerge from the calculations reported here pose particular difficulties for comparing calculated and experimental affinities. There are challenges in measuring the affinity of individual sites when there are multiple binding sites for the same ligand to compare with the site-specific values provided here. In addition, Cl^- is expected to be moving through the transporter, so equilibrium affinities may differ from steady-state affinity for transporter turnover. The cleanest experiments are carried out at high pH in mutated proteins, different conditions from the calculations reported here (16,17).

The calculated binding characterizes the competition of three anions for two binding sites. The binding is almost exclusively stabilized by the amide dipole potential in the helix cage, which is very localized, changing rapidly with position. Calculations of the affinity must compare the energy of the apo and bound states. The apo state is stabilized by clashes with E_x in S_x and Tyr_c and Ser_c in S_c, which are not well determined in the calculations reported here. The S_x affinity is particularly difficult to establish, as it requires calculating the energy of moving E_x from the position within the helix cage (APO) to the UP conformation, along with energy of proton binding to E_x. The CL_x affinity varies from being disallowed when E_x is in the APO position, to a modest proton-coupled Cl^- affinity when E_x is displaced from the center of the helix cage in MID structures, to the affinity being very tight if E_x starts in the UP position and the protein minimized with CL_x in the binding site. Thus, our calculations provide an estimate of how the helix cage and E_x position change ensures the coupling of proton and Cl^- binding. One piece of evidence that there are energy terms that are not included in the calculations is found in the analysis of Cl^- affinity in the E148Q mutant of CLC-ec1 (Table S6). Isothermal titration calorimetry measurements of Cl^- binding in this mutant, report that it binds Cl^- only ~10 times more tightly than the wild-type protein (16). In the calculations reported here, all of the work needed to protonate E_x in APO and move it to UP has already been paid in the E148Q mutant, so we calculate a very tight Cl^- affinity (Table S2). This calculated overstabilization of Cl^- binding to the prepared sites indicates that the true apo UP (Q148E) structure may be more stable than we expect here, so there is a larger cost we are missing to move the system to the conformation needed to bind Cl^-.

Our results are necessarily qualitative, as the Cl^- MC titrations occur with residue side chains sampling different rotamers and protonation states but with the backbone fixed very close to that of the parent x-ray structure. Minimizing the structure with neutral E_x increases the Cl^- binding affinity between 2 and 4 kcal/mol depending on the structure (Tables S2–S4), not unexpected as MD can greatly stabilize the input ionization state (47). In CE calculations it is not clear which value of the protein dielectric constant, which provides an implicit energy of relaxation on shifting Glu protonation state or Cl^- binding, is the "correct" one. In MCCE, the pairing of $e = 4$ and MC side-chain sampling has been benchmarked extensively (48). It can also be noted that analysis techniques that achieve similar values of proton or Cl^- affinity may break the energy down into different terms. Thus, our analysis provided relative importance of different elements of the structure, but an analysis with (for example) a different dielectric constant could provide similar affiliates but a different energy breakdown (40,48).

S_x and S_c, binding sites, located only ~4 Å apart, are formed by a helix cage, where the N-termini of helices F and N come together near the middle of the protein within the transmembrane region (Fig. 1). The backbone dipoles in the first two turns of the F and N helices provide a very electropositive hotspot that can accommodate two anions, be they E_x^{-1} with CL_c, or CL_x with CL_c (Fig. 5). CL_x and CL_c are almost equally stabilized by the helix cage

(Fig. 5), whereas E_x in the APO structure is less so, favoring Cl^- over E_x^{-1} in the competition for S_x (Table S6). The strongly localized electrostatic potential of the backbone dipoles allows the protein to tune the proton affinity of E_x by ~12 kcal/mol as the carboxyl group moves ~4 Å from the APO position within the helix cage via MID to its position in the UP structure (Fig. S6; Table S3).

The CLC transporters have been shown to have a 2 Cl^- to 1 proton stoichiometry of transport (3,5,6) and binding (17). The thermodynamic analysis of the Cl^- and proton affinity in structures with different orientations for E_x presented here shows how the CLC structure uses the competition of three anions for the helix cage electropositive region to obtain the $1H^+$:$2Cl^-$ stoichiometry (Fig. 7). The calculations support the experimental findings that E_x protonation is Cl^- induced (17,34). Here we see CL_x binding is strongly coupled to E_x protonation. In contrast, CL_c raises the E_x proton affinity, but not enough to bind a proton at pH 4.5. In addition, whereas the ionized E_x is strongly stabilized in the helix cage, the protonated residue has only a small penalty to leave the helix cage, permitting rotation to the position in UP structures.

The helix cage is a signature of the CLC fold and this built-in feature can explain why a wide range of exchangers with vastly different transport rates all have a 2:1 stoichiometry (3,10,49). The helix cage is not a protonatable motif, and when E_x is mutated to Ala or Gln, the protein will transport Cl^- but not protons (3,6,7,50). MCCE calculations show only limited proton uptake throughout the protein when Cl^- binds in the absence of E_x (as in E148A or E148Q, results not shown). The variation in E_x proton affinity helps explain why the experimentally determined Cl^- affinity is pH independent (9,16). Because the pK_a of E_x in APO structures is well below experimental pHs and that of E_x in UP structures with CL_x is above this pH range, the binding of 1 proton/2 Cl^- also appears pH independent. Conformational changes measured to be pH dependent (51–53) are independent of E_x as they are retained in the E148A mutant (52).

Stepwise model for coupled $2Cl^-$:$1H^+$ exchange

The calculated Cl^- affinities of S_x and S_c along with the H^+ affinity of E_x provide the state energies described in the thermodynamic cube for UP and MID structures (Fig. S7; Table S8), which was used to construct a model leading to the 2 Cl^-:$1H^+$ stoichiometry. This model (Fig. 8) takes into account the estimates for the state-to-state MID ↔ UP transitions (Fig. S7). The calculations suggest the $E_x^{-1}|CL_c$ state is the most stable (Fig. 7), in agreement with the Cl^- occupancy and E_x position found in the WT PDB: 1OTS structure.

One of the results of the strong positive potential of the helix cage is that the apo structure with only one charge in the binding region (E_x^{-1}) is at higher electrostatic energy than the states with two negative charges (Fig. 8). The states necessary for a stepwise translocation of 2 Cl^- ions into and out of the cage led to the mechanism depicted in Fig. 8. The apo state is needed in reaction cycles (27,49,51) that obtain the 2:1 stoichiometry without resorting to transient gating by extracellular Cl^- ions at the external site (Cl^- backflow) (6,50). Thus, the movement of Tyr_c and Ser_c, the intracellular light gate, into S_c as E_x moves into S_x are needed to produce a stable apo state. These intra-S_c conformations are found in the PDB: 2EXW APO structure (Fig. S2). In small side-chain mutants of Tyr_c, more than 2 Cl^-/proton

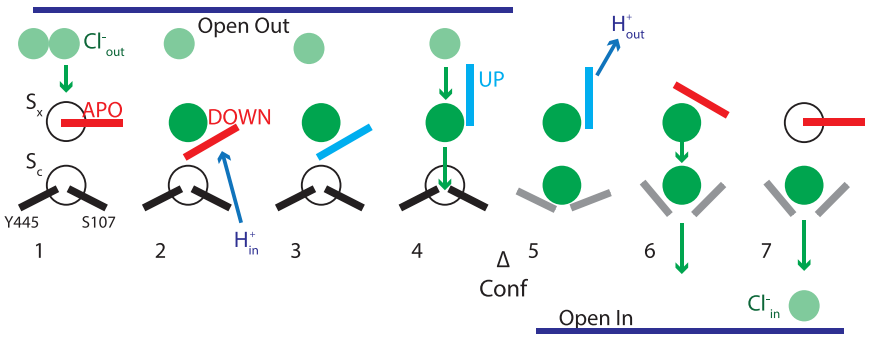

FIGURE 8 Stepwise model for $2Cl^-$:$1H^+$ exchange in the Cl^- inflow/H^+ outflow direction. Shown here are the states of the exchange cycle. Red or blue bar denotes E_x in its ionized or neutral state in different orientations; S_x and S_c are the open or solid (*green*) binding sites; lighter-green circles are unbound Cl ions. Black and gray bars denote residues of the inner gate, Ser_c (S107) and Tyr_c (Y445). States 2–4 constitute the outward-facing, ion-loading phase of the cycle followed by Cl^- release in the inward-facing States 6 and 7. The model includes substrate-dependent domain-level (*heavy gate*) conformational changes (ΔConf), allowing contact with either the outer or inner compartment (21–23). Side-chain (*light gate*) movements of E_x, Tyr_c, and Ser_c, shown by changes in the positions of their representative lines, control access to individual sites (24). The accessibility switch is proposed to be triggered by having Cl^- at both S_x and S_c (State 5). [1] The model starts in the apo state where side chains of the light gates block both sites. A conformational change of the outer gate allows Cl^- entry. Repulsion by the approaching Cl^- moves the ionized E_x side chain to the DOWN position where it binds a proton from the inside; [3] this results in S_x filled and E_x protonated. [4] The coupled protonation of E_x from the inside with Cl^- binding at the external site moves E_x into the UP position. [5] After translocation of the ion from the external to central site, another ion binds the newly vacated external site. This yields the most favorable configuration, with 2 Cl ions and protonated E_x UP. [6] The fully loaded state constitutes a gate-coordination signal for the outer gates to close and the inner one to open, allowing release of the first Cl^- to the intracellular side with concurrent release of H^+ to the outside and movement of the ionized E_x toward the helix cage. [7] Another ion translocation takes place to release the second Cl^-. E_x returns to the APO position. [1] The high cost of unbinding the central site is reduced by reentry of the inner gate Ser_c and Tyr_c into the central site to reform.

are transported (13), suggesting that in the absence of a closed, apo state, Cl^- can sneak through the protein without being tightly coupled to proton transport. In addition, the rather small difference in energy when E_x is rotated outwards in UP structures may make it easier for CL_x to move to S_c. The higher proton affinity of E_x when it is out of the helix cage suggests it could become protonated early in the cycle and remain so until the apo state is reformed at the end of the cycle.

In all structures studied here, S_x is not visible to the surface. Some domain-level components (or heavy gates), involving more significant conformational changes than the movement of light gates (E_x, Ser_c, and Tyr_c), must open to allow entry of Cl^- in the extracellular vestibule (between states 1 and 2 in Fig. 8). A larger change between the outward-facing, occluded ($OF_{occluded}$) and the outward-facing, open (OF_{open}) conformations recently proposed in a multipronged, NMR/MD simulation study of conformations in CLC-ec1 (27), is proposed to occur when both S_x and S_c are filled. Domain-level motions have been detected either in vitro (51–55) or by simulations (56,57). Given the localization of the electropositive potential created by the helix cage (Fig. S1 *b*), small changes in the helical alignment can be used in the cycle to modulate Cl^- affinity, helping to bind and release Cl^- and protons.

CONCLUSIONS

The thermodynamic analysis of ion and proton binding shows how the structure of the CLC transporter effects the pH-independent, 2 Cl^- to 1 proton binding stoichiometry. The key features are a helix cage, which creates a compact region with a very strong electropositive potential that stabilizes two anions and a single Glu that competes with two Cl ions (Fig. S1; Table 2). The helix cage plus E_x creates a robust affinity switch, as can be seen in the change of the apo pK_a value of E_x from negative values when it is in the cage (APO or MID), to values close to the physiological pH of 4.5 when it moves out of it, to the position found in the reversed E148Q mutant (UP) structure (Fig. S6; Table 1). As proton and Cl^- binding at S_x are thermodynamically linked (Fig. 4), a favorable change in E_x proton affinity is accompanied by a similar change in Cl^- affinity, as the electropositive cage favors anions.

Although the helix cage can support Cl^- binding without protons, as in the E148A and E148Q mutants, the introduction of E_x causes C^-binding to be coupled to no more than one proton ensuring 2:1 stoichiometry. The presence of E_x weakens Cl^- binding, either by the penalty to bind a proton and move E_x^0 out of the helix cage when Cl^- binds S_x, or by the E_x^{-1}:Cl^- repulsion as the central site is filled. As this energy is paid with the first Cl^- bound, the second can bind more strongly than expected given the repulsion between the Cl^- in the closely spaced binding sites. The interaction of E_x with the helix cage and the Cl^- ion also explains why protonation of the gating Glu is essentially pH independent. Because the pK_a of E_x is <0 in the apo structure and >7 when Cl^- is bound, the solution pH does not influence the protonation of the light gate as these limits are above and below the range of most experiments.

SUPPORTING MATERIAL

Supporting Materials and Methods, seven figures, and eight tables are available at http://www.biophysj.org/biophysj/supplemental/S0006-3495(17)30850-0.

AUTHOR CONTRIBUTIONS

C.C. performed the simulations for this research designed by C.C. and M.R.G. Both C.C. and M.R.G. analyzed the data and wrote the manuscript.

ACKNOWLEDGMENTS

We thank Dr. Alessio Accardi and Dr. Themis Lazaridis for generously sharing their insights on this subject.

Research was funded by grant No. MCB-1519640 from the National Science Foundation (NSF). M.R.G. also acknowledges infrastructure support from the National Institute on Minority Health and Health Disparities (grant No. 8G12MD007603) from the National Institutes of Health (NIH).

SUPPORTING CITATIONS

References (58–64) appear in the Supporting Material.

REFERENCES

1. Jentsch, T. J. 2008. CLC chloride channels and transporters: from genes to protein structure, pathology and physiology. *Crit. Rev. Biochem. Mol. Biol.* 43:3–36.
2. Schwab, A., A. Fabian, …, C. Stock. 2012. Role of ion channels and transporters in cell migration. *Physiol. Rev.* 92:1865–1913.
3. Accardi, A., and C. Miller. 2004. Secondary active transport mediated by a prokaryotic homologue of ClC Cl^- channels. *Nature.* 427:803–807.
4. Scheel, O., A. A. Zdebik, …, T. J. Jentsch. 2005. Voltage-dependent electrogenic chloride/proton exchange by endosomal CLC proteins. *Nature.* 436:424–427.
5. Picollo, A., and M. Pusch. 2005. Chloride/proton antiporter activity of mammalian CLC proteins ClC-4 and ClC-5. *Nature.* 436:420–423.
6. Feng, L., E. B. Campbell, …, R. MacKinnon. 2010. Structure of a eukaryotic CLC transporter defines an intermediate state in the transport cycle. *Science.* 330:635–641.
7. Dutzler, R., E. B. Campbell, …, R. MacKinnon. 2002. X-ray structure of a ClC chloride channel at 3.0 Å reveals the molecular basis of anion selectivity. *Nature.* 415:287–294.
8. Dutzler, R., E. B. Campbell, and R. MacKinnon. 2003. Gating the selectivity filter in ClC chloride channels. *Science.* 300:108–112.
9. Lobet, S., and R. Dutzler. 2006. Ion-binding properties of the ClC chloride selectivity filter. *EMBO J.* 25:24–33.
10. Zdebik, A. A., G. Zifarelli, …, M. Pusch. 2008. Determinants of anion-proton coupling in mammalian endosomal CLC proteins. *J. Biol. Chem.* 283:4219–4227.

11. Nguitragool, W., and C. Miller. 2007. CLC Cl^-/H^+ transporters constrained by covalent cross-linking. *Proc. Natl. Acad. Sci. USA.* 104:20659–20665.
12. Robertson, J. L., L. Kolmakova-Partensky, and C. Miller. 2010. Design, function and structure of a monomeric ClC transporter. *Nature.* 468: 844–847.
13. Walden, M., A. Accardi, …, C. Miller. 2007. Uncoupling and turnover in a Cl^-/H^+ exchange transporter. *J. Gen. Physiol.* 129:317–329.
14. Jayaram, H., A. Accardi, …, C. Miller. 2008. Ion permeation through a Cl^--selective channel designed from a CLC Cl^-/H^+ exchanger. *Proc. Natl. Acad. Sci. USA.* 105:11194–11199.
15. Accardi, A., S. Lobet, …, R. Dutzler. 2006. Synergism between halide binding and proton transport in a CLC-type exchanger. *J. Mol. Biol.* 362:691–699.
16. Picollo, A., M. Malvezzi, …, A. Accardi. 2009. Basis of substrate binding and conservation of selectivity in the CLC family of channels and transporters. *Nat. Struct. Mol. Biol.* 16:1294–1301.
17. Picollo, A., Y. Xu, …, A. Accardi. 2012. Synergistic substrate binding determines the stoichiometry of transport of a prokaryotic H^+/Cl^- exchanger. *Nat. Struct. Mol. Biol.* 19:525–531, S1.
18. Aqvist, J., H. Luecke, …, A. Warshel. 1991. Dipoles localized at helix termini of proteins stabilize charges. *Proc. Natl. Acad. Sci. USA.* 88: 2026–2030.
19. Faraldo-Gómez, J. D., and B. Roux. 2004. Electrostatics of ion stabilization in a ClC chloride channel homologue from *Escherichia coli*. *J. Mol. Biol.* 339:981–1000.
20. Ko, Y. J., and W. H. Jo. 2010. Chloride ion conduction without water coordination in the pore of ClC protein. *J. Comput. Chem.* 31:603–611.
21. Cohen, J., and K. Schulten. 2004. Mechanism of anionic conduction across ClC. *Biophys. J.* 86:836–845.
22. Forrest, L. R., and G. Rudnick. 2009. The rocking bundle: a mechanism for ion-coupled solute flux by symmetrical transporters. *Physiology (Bethesda).* 24:377–386.
23. Radestock, S., and L. R. Forrest. 2011. The alternating-access mechanism of MFS transporters arises from inverted-topology repeats. *J. Mol. Biol.* 407:698–715.
24. Forrest, L. R., R. Krämer, and C. Ziegler. 2011. The structural basis of secondary active transport mechanisms. *Biochim. Biophys. Acta.* 1807: 167–188.
25. Jardetzky, O. 1966. Simple allosteric model for membrane pumps. *Nature.* 211:969–970.
26. Drew, D., and O. Boudker. 2016. Shared molecular mechanisms of membrane transporters. *Annu. Rev. Biochem.* 85:543–572.
27. Khantwal, C. M., S. J. Abraham, …, M. Maduke. 2016. Revealing an outward-facing open conformational state in a CLC Cl^-/H^+ exchange transporter. *eLife.* 5:e11189.
28. Traverso, S., G. Zifarelli, …, M. Pusch. 2006. Proton sensing of CLC-0 mutant E166D. *J. Gen. Physiol.* 127:51–65.
29. Zifarelli, G., S. De Stefano, …, M. Pusch. 2012. On the mechanism of gating charge movement of ClC-5, a human Cl^-/H^+ antiporter. *Biophys. J.* 102:2060–2069.
30. Vien, M., D. Basilio, …, A. Accardi. 2017. Probing the conformation of a conserved glutamic acid within the Cl^- pathway of a CLC H^+/Cl^- exchanger. *J. Gen. Physiol.* 149:523–529.
31. Bisset, D., B. Corry, and S.-H. Chung. 2005. The fast gating mechanism in ClC-0 channels. *Biophys. J.* 89:179–186.
32. Lee, S., H. B. Mayes, …, G. A. Voth. 2016. The origin of coupled chloride and proton transport in a Cl^-/H^+antiporter. *J. Am. Chem. Soc.* 138:14923–14930.
33. Cheng, M. H., and R. D. Coalson. 2012. Molecular dynamics investigation of Cl^- and water transport through a eukaryotic CLC transporter. *Biophys. J.* 102:1363–1371.
34. Bostick, D. L., and M. L. Berkowitz. 2004. Exterior site occupancy infers chloride-induced proton gating in a prokaryotic homolog of the ClC chloride channel. *Biophys. J.* 87:1686–1696.
35. Kieseritzky, G., and E. W. Knapp. 2011. Charge transport in the ClC-type chloride-proton anti-porter from *Escherichia coli*. *J. Biol. Chem.* 286:2976–2986.
36. Han, W., R. C. Cheng, …, E. Tajkhorshid. 2013. Water access points and hydration pathways in CLC H^+/Cl^- transporters. *Proc. Natl. Acad. Sci. USA.* 111:1819–1824.
37. Jiang, T., W. Han, …, E. Tajkhorshid. 2016. Molecular basis for differential anion binding and proton coupling in the Cl^-/H^+exchanger ClC-ec1. *J. Am. Chem. Soc.* 138:3066–3075.
38. Nguitragool, W., and C. Miller. 2006. Uncoupling of a CLC Cl^-/H^+ exchange transporter by polyatomic anions. *J. Mol. Biol.* 362:682–690.
39. Yin, J., Z. Kuang, …, T. L. Beck. 2004. Ion transit pathways and gating in ClC chloride channels. *Proteins.* 57:414–421.
40. Song, Y., J. Mao, and M. R. Gunner. 2009. MCCE2: improving protein pK_a calculations with extensive side chain rotamer sampling. *J. Comput. Chem.* 30:2231–2247.
41. Song, Y., and M. R. Gunner. 2009. Using multiconformation continuum electrostatics to compare chloride binding motifs in α-amylase, human serum albumin, and Omp32. *J. Mol. Biol.* 387:840–856.
42. Song, Y., and M. R. Gunner. 2014. Halorhodopsin pumps Cl^- and bacteriorhodopsin pumps protons by a common mechanism that uses conserved electrostatic interactions. *Proc. Natl. Acad. Sci. USA.* 111: 16377–16382.
43. Iyer, R., T. M. Iverson, …, C. Miller. 2002. A biological role for prokaryotic ClC chloride channels. *Nature.* 419:715–718.
44. Mao, J., K. Hauser, and M. R. Gunner. 2003. How cytochromes with different folds control heme redox potentials. *Biochemistry.* 42:9829–9840.
45. Hess, B., C. Kutzner, …, E. Lindahl. 2008. GROMACS4: algorithms for highly efficient, load-balanced, and scalable molecular simulation. *J. Chem. Theory Comput.* 4:435–447.
46. Hornak, V., R. Abel, …, C. Simmerling. 2006. Comparison of multiple Amber force fields and development of improved protein backbone parameters. *Proteins.* 65:712–725.
47. Zheng, Y., and Q. Cui. 2017. Microscopic mechanisms that govern the titration response and pK_a values of buried residues in staphylococcal nuclease mutants. *Proteins.* 85:268–281.
48. Gunner, M. R., X. Zhu, and M. C. Klein. 2011. MCCE analysis of the pK_as of introduced buried acids and bases in staphylococcal nuclease. *Proteins.* 79:3306–3319.
49. Miller, C., and W. Nguitragool. 2009. A provisional transport mechanism for a chloride channel-type Cl^-/H^+ exchanger. *Philos. Trans. R. Soc. Lond. B Biol. Sci.* 364:175–180.
50. Feng, L., E. B. Campbell, and R. MacKinnon. 2012. Molecular mechanism of proton transport in CLC Cl^-/H^+ exchange transporters. *Proc Natl Acad Sci U S A.* 109:11699–11704.
51. Elvington, S. M., C. W. Liu, and M. C. Maduke. 2009. Substrate-driven conformational changes in ClC-ec1 observed by fluorine NMR. *EMBO J.* 28:3090–3102.
52. Abraham, S. J., R. C. Cheng, …, M. Maduke. 2015. ^{13}C NMR detects conformational change in the 100-kD membrane transporter ClC-ec1. *J. Biomol. NMR.* 61:209–226.
53. Bell, S. P., P. K. Curran, …, J. A. Mindell. 2006. Site-directed fluorescence studies of a prokaryotic ClC antiporter. *Biochemistry.* 45:6773–6782.
54. Jayaram, H., J. L. Robertson, …, C. Miller. 2011. Structure of a slow CLC Cl^-/H^+ antiporter from a cyanobacterium. *Biochemistry.* 50: 788–794.
55. Basilio, D., K. Noack, …, A. Accardi. 2014. Conformational changes required for H^+/Cl^- exchange mediated by a CLC transporter. *Nat. Struct. Mol. Biol.* 21:456–463.
56. Miloshevsky, G. V., A. Hassanein, and P. C. Jordan. 2010. Antiport mechanism for Cl^-/H^+ in ClC-ec1 from normal-mode analysis. *Biophys. J.* 98:999–1008.

57. Krivobokova, T., R. Briones, …, B. L. de Groot. 2012. Partial least-squares functional mode analysis: application to the membrane proteins AQP1, Aqy1, and CLC-ec1. *Biophys. J.* 103:786–796.

58. Cornell, W. D., P. Cieplak, …, P. A. Kollman. 1995. A second generation force field for the simulation of proteins, nucleic acids, and organic molecules. *J. Am. Chem. Soc.* 117:5179–5197.

59. Alexov, E., and M. R. Gunner. 1997. Incorporating protein conformational flexibility into the calculation of pH-dependent protein properties. *Biophys. J.* 72:2075–2093.

60. Georgescu, R. E., E. G. Alexov, and M. R. Gunner. 2002. Combining conformational flexibility and continuum electrostatics for calculating pK_as in proteins. *Biophys. J.* 83:1731–1748.

61. Nicholls, A., and B. Honig. 1991. A rapid finite difference algorithm utilizing successive over-relaxation to solve the Poisson-Boltzmann equation. *J. Comput. Chem.* 12:435–445.

62. Sitkoff, D., K. A. Sharp, and B. Honig. 1994. Accurate calculation of hydration free-energies using macroscopic solvent models. *J. Phys. Chem.* 98:1978–1988.

63. Jensen, K. P., and W. L. Jorgensen. 2006. Halide, ammonium, and alkali metal ion parameters for modeling aqueous solutions. *J. Chem. Theory Comput.* 2:1499–1509.

64. Rashin, A. A., and B. Honig. 1985. Reevaluation of the Born model of ion hydration. *J. Phys. Chem.* 89:5588–5593.